Journal of Materials Chemistry A

PAPER

View Article Online
View Journal | View Issue

Cite this: J. Mater. Chem. A, 2014, 2, 8472

Sulfur-rich carbon cryogels for supercapacitors with improved conductivity and wettability†

Yao Zhou,[abc] Stephanie L. Candelaria,[b] Qian Liu,[a] Yunxia Huang,[d] Evan Uchaker[b] and Guozhong CaO*[b]

Received 20th February 2014
Accepted 25th March 2014

DOI: 10.1039/c4ta00894d

www.rsc.org/MaterialsA

Sulfur-rich carbon cryogels derived from 2-thiophenecarboxaldehyde and resorcinol were synthesized through sol–gel processing, which demonstrated good stability with less than 4% capacitance loss after 1000 charge–discharge cycles. Pyrolysis of sulfur-rich carbon at higher temperatures resulted in decreased electrical conductivity, which was caused by the degree of graphitization deteriorating at high temperatures. An increased amount of sulfur can effectively improve the wetting behavior of the carbon electrode in organic electrolytes. Specifically, when the sulfur content is 2.5 at%, the electrode was completely wetted. Additionally, pseudocapacitive reactions introduced from sulfur were observed in this electrolyte. Synergistic effects of sulfur and pore structure controlled the final electrochemical properties. The sulfur-containing sample pyrolyzed at 1000 °C had the best specific capacitance and impedance performance. When activated in air without sol–gel processing optimization, the sulfur-modified carbon demonstrated a capacitance of 94.4 F g^{-1} in organic electrolytes.

1 Introduction

Supercapacitors have been extensively investigated for decades due to the exponential growth of demand for portable electric devices and hybrid electric vehicles.[1,2] They can serve as backup energy devices to batteries due to their higher power density. Generally, supercapacitors can be classified into two categories on the basis of their energy storage mechanism.[3] One category is based on the formation of an electrical double layer, and the other relies on pseudo-redox reactions. For electrical double layer supercapacitors, the electrical energy is stored as pure electrostatic charge accumulated at the interface of the electrode/electrolyte.[4] Performance is strongly dependent on the pore structure including the surface area, pore size and pore size distribution; hence, porous carbons with a large specific surface area and controlled pore structure are highly recommended.[5,6] For pseudo-redox reaction based supercapacitors, the electrical energy is stored in the form of chemical potential through pseudocapacitive electron transfer between the electrode and the electrolyte. Transition metal oxides (RuO_2, NiO, *etc.*), functional groups on the carbon-matrix material, and conductive polymers are all candidates for redox reactions.[7–10] However, both metal oxides and conductive polymers often exhibit poor cyclic stability, which limits their practical application.[11–13]

The introduction of foreign elements in highly porous carbon is considered to be a feasible method to combine the advantages of high surface area carbon and pseudocapacitance induced by the heteroatom.[14] Porous carbon modified with foreign elements has been proved to be physicochemically stable with enhanced capacitance, wettability and electrical conductivity.[15] Some recent researchers concentrated on oxygen substitution into the graphene layers of the carbon network. For example, Jurewicz[16] reported that electron donor characteristics were introduced to the carbon network after oxygen modification in an aqueous electrolyte and the capacitance increased. However, oxygen heteroatoms have proven to be detrimental when used in organic electrolytes due to irreversible reactions between oxygen and the electrolyte ions. Porous carbon modified with nitrogen functional groups or nitrogen heteroatoms has attracted much interest as well because nitrogen functional groups contribute to pseudocapacitance through faradaic reactions in both aqueous[17,18] and organic electrolytes.[19,20] Nitrogen modification was also found to improve the wettability of the carbon network.[21] Recently, the negative impact of nitrogen heteroatoms on organic electrolytes was also reported.[22] Phosphorus-enriched carbons are also found to have increased specific capacitance compared to non-modified carbons while phosphorus readily evaporates even at room temperature which makes modified phosphorus unstable.[6]

Sulfur, similar to oxygen, nitrogen and phosphorus, has lone-pair electrons and may be able to introduce

[a]The State Key Laboratory of High Performance Ceramics and Superfine Microstructure, Shanghai Institute of Ceramics, Chinese Academy of Sciences, 1295 Dingxi Road, Shanghai, 200050, China

[b]Department of Materials Science and Engineering, University of Washington, Seattle, WA 98195, USA. E-mail: gzcao@u.washington.edu; Fax: +1-206-543-3100; Tel: +1-206-616-9084

[c]University of Chinese Academy of Sciences, 19A Yuquan Road, Beijing, 100049, China

[d]School of Technical Physics, Xidian University, Xi'an 710071, China

† Electronic supplementary information (ESI) available. See DOI: 10.1039/c4ta00894d

pseudocapacitance to carbon. Hasegawa[23] was the first to report that sulfur-containing carbon could be used in supercapacitors. Macro/meso/microporous carbon monolith electrodes doped with sulfur from sulfonated poly(divinylbenzene) (PDVB) were prepared with concentrated sulphuric acid and CO_2 activation at 1000 °C for supercapacitors in an aqueous system. The small humps that appeared in cyclic voltammetry curves were attributed to the pseudocapacitance introduced by sulfur in the aqueous electrolyte system. In addition, resorcinol and thioldiphenol were employed as precursors to prepare mesoporous carbon doped with sulfide, sulfoxide, and sulfone functional groups.[24] Specific capacitance was improved by 38% in the aqueous system compared to that of conventional ordered mesoporous carbon due to the enlarged dielectric constant and a series of redox faradic reactions provided by the additional sulfone and sulfoxide species.

Organic electrolytes can provide a higher working voltage range compared to that in an aqueous system, which can lead to enhanced energy density. Additionally, the electrical conductivity and wettability of sulfur-containing porous carbon were not taken into account in previous research studies. These two aspects are essential to the final electrochemical performance.[25,26] Good electrical conductivity can shorten paths of electron transport which in turn improves capacitive performance;[27] wetting behavior between the electrolyte and the surface of carbon shows whether the surface functional groups are electrolyte-phobic or electrolyte-philic, which indicates to some extent the penetration of the electrolyte into the porous carbon material.[28] Recently, Huang[29] reported that sulfur-modified activated carbon in organic electrolytes shows improvement in electric conductivity and capacitance can reach up to 82.3 F g^{-1}. However, the mechanism of the sulfur impact on electric conductivity has not been studied yet.

In this study, sulfur-rich porous carbon cryogels were synthesized through the sol–gel processing with resorcinol and sulfur-containing 2-thiophenecarboxaldehyde as precursors, and with the assistance of the surfactant ethylene oxide/propylene oxide block copolymer (F127). This porous carbon was used as an electrode for supercapacitors with an organic electrolyte consisting of 1 M tetraethylammonium tetrafluoroborate (TEATFB) in 50–50 propylene carbonate–dimethylcarbonate (PC–DMC). The chemical composition and pore structure were tested using X-ray photoelectron spectroscopy (XPS) and nitrogen adsorption analysis, respectively. Electrochemical properties were characterized by means of cyclic voltammetry, galvanic cycling, and electrochemical impedance spectroscopy. Additionally, the effects of sulfur on wettability and electrical conductivity are discussed in detail.

2 Experimental

2.1 Synthesis of 2-thiophenecarboxaldehyde derived mesoporous carbons (TCs) and reference resorcinol-formaldehyde (RF) derived pure carbon

To prepare TC-denoted sulfur-containing mesoporous carbons, 1.2626 g (0.01 mol) resorcinol was dissolved in a solution containing 7.0 g of DI water, 7.0 g of ethanol and 1.75 g of ethylene oxide/propylene oxide block copolymer (F127) as a surfactant under magnetic stirring until the solution turned transparent. After that, 0.0644 g of hexamine was added as the catalyst to the above solution, which was kept under stirring for an additional 1 h. Then 1.075 mL (0.01 mol) of 2-thiophenecarboxaldehyde was added under an additional 1 h stirring. The mixture was sealed and cured in an oven at 80 °C for 4 days to allow for gelation and aging to strengthen the newly formed three-dimensional gel network. The resultant gels were subsequently freezed and dried in a vacuum at −50 °C in a Labconco Free-Zone 1 L freeze dryer for three days. The dried samples were heated in a N_2 atmosphere at 350 °C for 3 h to remove the surfactant F127. The surfactant-free samples were pyrolyed in nitrogen at a temperature of either 775, or 900, or 1000, or 1200 °C for 3 h with a ramp rate of 5 °C min^{-1}. These samples are referred to as TC775, TC900, TC1000 and TC1200, respectively.

Due to the usage of a sulfur-containing precursor as a sulfur source instead of added sulfur-containing chemical separately, it is hard to remove all sulfur from the carbon matrix. In order to make pure carbon with similar morphology to the reference, RF derived porous carbon was prepared according to the process reported by Garcia,[30] with freeze drying and pyrolysis in N_2 without activation in CO_2. The preparation of a pure carbon sample is briefly reiterated here: the formaldehyde to resorcinol molar ratio was set to 2.0 and the ratio of resorcinol to the catalyst (Na_2CO_3) used in the experiment was 75. The resorcinol to water ratio was fixed at 0.25. The sample was pyrolyzed at 1000 °C for 3 h to compare with the properties of sample TC1000.

2.2 Characterization

X-ray photoelectron spectroscopy (XPS) was used to determine the sulfur content and surface functional groups of the samples. Spectra were taken on a Surface Science Instruments S-probe spectrometer. The X-ray spot size for these acquisitions was approximately 800 μm and the take-off angle was 55°, corresponding to a sampling depth of approximately 50–70 Å. Data analyses were carried out using the Service Physics ESCA Hawk 7 Data Analysis Software (Service Physics, Bend, OR). Three spots were measured on each sample to make final results credible.

N_2 adsorption and desorption isotherms were obtained at −196 °C on a Micromeritics Tristar 3000 system. Samples were degassed at 100 °C under vacuum for at least 6 h prior to measurement. The total surface area was determined using the multipoint Brunauer–Emmett–Teller (BET) method. For the mesopore surface area, pore volume, and pore diameter, the Barrett–Joyner–Halenda (BJH) method was used, but the specific surface area and the pore volume of micropores were calculated using the *t*-method. Each sample was measured three times.

Surface morphologies of pores were observed by field emission scanning electron microscopy (FESEM, FEI Magellan 400, 5.00 kV). The electrical conductivities of samples were measured using a four point probe instrument. Raman spectra were taken with an excitation wavelength of 532 nm. Typically three spectra were taken for each sample to ensure uniformity.

Contact angles were measured with the static sessile drop method using a VCA Optima goniometer. All measurements were performed with TCs and RF powder samples mixed with 3.0 wt% binder polytetrafluoroethylene (PTFE) that had been rolled into sheets with a thickness of 60 μm. Surfaces were wet with approximately 1 μL of 1 M tetraethylammonium tetrafluoroborate (TEATFB) in saturated 50–50 propylene carbonate (PC)–dimethylcarbonate (DMC) and analyzed immediately after the droplet touched the as-prepared sheets. Each sample underwent measurements in five different spots. VCA OptimaXE software was used to measure angles on the left side of the droplet and the average angle was calculated.

2.3 Electrochemical analyses

Electrodes were prepared by grinding the samples into a fine powder followed by mixing with 3.0 wt% binder PTFE. The resulting mixture was rolled into sheets and then punched out with a thickness of 60 μm and a diameter of 10 mm. A Celgard® porous film separates the electrodes and special carbon coated aluminum contacts were used because coating carbon contacts instead of aluminum with tested porous carbon can reduce the interfacial effect between contacts and electrodes. TEATFB in saturated 50–50 PC–DMC was used as an electrolyte. To test the electrodes, symmetrical two-electrode coin cells were assembled in argon. The cells were placed under vacuum to increase the penetration of the electrolyte into the pores of carbon electrodes. It is found that 1.5 h evacuation at −20 MPa is required to ensure thorough or complete electrolyte penetration, which is needed to ensure the true electrochemical properties characterized (Fig. S1†). A time longer than 1.5 h makes little difference and is not needed.

Cyclic voltammograms (CV) and galvanic cycle (GC) curves were measured by means of a Solartron 1287A with a voltage ranging between 0 and 2 V. The CVs were measured at a scan rate of 10 mV s^{-1}. A current load of 0.5 A g^{-1} was applied in GC measurements. Electrochemical impedance spectroscopic analyses were carried out using the Solartron 1287A in conjunction with a Solartron 1260FRA/impedance analyzer. A frequency range between 0.1 MHz and 1 MHz and a 10 mV AC voltage were used for this scan. The specific capacitance in Farad per gram (F g^{-1}) was calculated from the discharge slope during galvanic cycles according to the following equation:

$$C_{\text{spec}} = 4I\Delta t/\Delta Vm \quad (1)$$

where I is the discharge current in amps, Δt is the discharge time in seconds, ΔV is the discharge voltage in volts, and m is the total mass of the active materials in both electrodes in grams.

3 Results and discussion

3.1 Composition and pore structure

XPS measurements were applied to determine the atomic composition and chemical state of sulfur in the carbon network. Fig. 1 shows the high-resolution XPS spectra of C 1s and S 2p for sample TC1000. Other TC samples had similar S 2p spectra (Fig. S2†). The binding energy scales of the spectra were calibrated by assigning the most intense C 1s peak a binding energy of 285.0 eV. Fig. 1b shows that the TC1000 sample exhibited two peaks at 164.0 eV and 165.2 eV, which were assigned to S $2p_{3/2}$ and S $2p_{1/2}$, respectively, of thiophene-like sulfur incorporated into the graphite structure.[31] The separation of S $2p_{3/2}$ and S $2p_{1/2}$ peaks is 1.2 eV, agreeing well with the expected value of 1.18 eV for this spin–orbit doublet.[32] There are no other peaks of S 2p which implies the single and homogeneous status of the sulfur species in the sulfur-containing carbon.

The content of sulfur in the TC samples decreased from 2.5 ± 0.1 at% to 0.5 ± 0.1 at% when the pyrolysis temperature rose from 775 °C to 1200 °C (Table 1). Pyrolysis of TC samples with increasing temperatures results in increased desulfurization, as more sulfur in the carbon network forms gaseous H_2S and CS_2 under a N_2 atmosphere at temperatures higher than 500 °C.[33–35] The oxygen content was found to decrease with an increased pyrolysis temperature. For example, sample TC900 possessed 5.5 ± 0.4 at% oxygen, while sample TC775 had 23% more oxygen. However, further increasing temperatures higher than 900 °C had little effect on the reduction of oxygen. One explanation is that the surface oxygen in carbon cryogel is weakly bonded and can be readily removed. The surface oxygen would be removed at ~900 °C while the remaining bulk oxygen embedded inside the carbon network is hard to remove even at high temperatures.

Surfactant F127 has no elemental effect on the final products. After organic cryogels underwent the heat treatment at 350 °C for 3 h, all surfactant (F127) was removed. TGA measurement (Fig. S3†) showed that the weight loss of pure F127 after heat treatment at 350 °C for 3 h was 100%, indicating that there was no residue from F127 in the final carbon cryogels.

The whole synthetic process involves a facile aqueous self-assembly coupled with a carbonization strategy. F127 was employed as the structure directing agent for polymerization. 2-Thiophenecarboxaldehyde polymerizes with resorcinol, and free hydroxyl groups in benzene rings could assemble with F127 *via* hydrogen bonds and form a meso-structure.[36,37]

Nitrogen sorption isotherms for samples TC775, TC900, TC1000 and TC1200 are shown in Fig. 2a. The four samples exhibit type IV isotherms with shapes between the so-called H2 and H4 type hysteresis loops.[38] It is believed that the H2 type is explained as the consequence of regular "bottle like" pores which exhibit a smaller sized opening but a larger sized inside chamber, while H4 is associated with the existence of narrow slit-like pores. With lower pyrolysis temperature, the hysteresis loop ended at higher relative pressures (P/P_0) but there was no sorption increase when P/P_0 = 0.9–1.0, indicating increased mesopore size but without appearance of macropores.[39] In all four samples, diverged desorption isotherms at relative low pressures were observed, an indication of existence of a considerable amount of micropores.

The nitrogen sorption data of TC775, TC900, TC1000 and TC1200 are summarized in Table 2, including the surface area, pore volume of mesopores and micropores, pore size of mesopores and total specific surface area. With increased temperatures, volumes and pore sizes of mesopores correspondingly

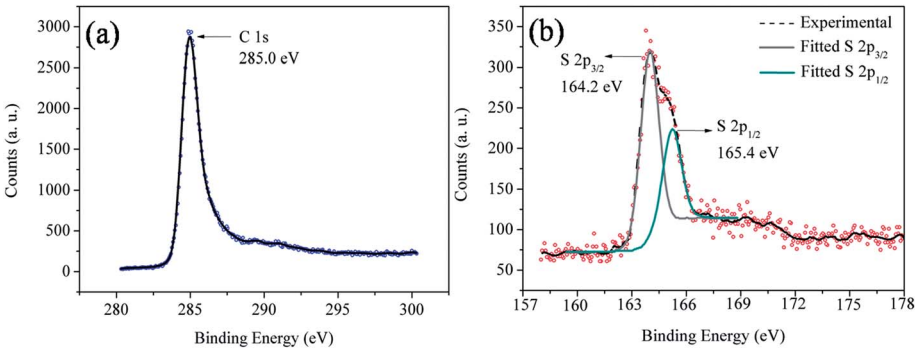

Fig. 1 High resolution XPS spectrum of C 1s and S 2p for the sulfur-rich carbon cryogel pyrolyzed at 1000 °C for 3 h.

Table 1 Compositional data from XPS

Sample ID	S atomic%	O	C
TC775	2.5 ± 0.1	7.1 ± 0.3	90.4 ± 0.3
TC900	1.9 ± 0.1	5.5 ± 0.4	92.6 ± 0.4
TC1000	1.4 ± 0.1	5.1 ± 0.1	93.5 ± 0.1
TC1200	0.5 ± 0.1	5.0 ± 0.1	94.5 ± 0.2

increased. The increased amount of mesopores may be caused by micropore merging. A manifested peak at 2.1 nm in TC1200 could be observed in Fig. 2b, which was much sharper than that of samples TC1000 and TC900. These data indicated that higher temperatures facilitated the growth of micropores into mesopores. Furthermore, when temperatures rose, the average pore size of mesopores increased from 3.2 nm (TC775) to 4.3 nm (TC1200) and the mesopore size distribution shifted to larger sizes. SEM of pore morphologies also supported these findings. From Fig. 3, pores were clearly observed and the pore size gradually increased with rising temperatures without appreciable change to the pore morphology. The enlarged mesopore size and volume are advantageous for energy storage since large pore channels permit rapid electrolyte transport. Additionally, the specific surface area also increased with rising pyrolysis temperatures even though the pore size increased. It can be observed that the micropore surface had a gradual increase from sample TC775 to TC1200 indicating that a great amount of micropores formed caused by high pyrolysis temperature. These newly formed micropores compared to that at lower temperature contributed to the enlarged specific surface area. The higher temperature was necessary to remove unwanted functional groups more completely which in turn could open up the closed micropores.[20]

3.2 Electrical conductivity

The four point probe method was employed to measure the electrical conductivity of the TC samples. Since it is difficult to form intact sheets with the as-prepared carbon powder without a binder, all measurements were performed with samples that had been rolled into 0.12 mm thick sheets with 30 mg porous carbon powder and 3 wt% PTFE. The values of electrical conductivity of the samples were much lower than data reported previously[40] due to the addition of the non-conductive binder PTFE. Fig. 4a illustrates the conductivity change trend of TC775, TC900, TC1000 and TC1200 samples. TC775, which is pyrolyzed at 775 °C, showed the highest electrical conductivity (2.10 ± 0.15 S cm^{-1}). With increased pyrolysis temperature, the values of electrical conductivity of the TC samples gradually decreased. It should be noted that densities of samples except TC1200 were nearly the same (Fig. S4†) even though differences existed in the values for the specific surface area, indicating that the change in electrical conductivity of samples TC775, TC900 and TC1000 was not mainly affected by density. The nearly doubled pore volume of TC1200 compared to other samples definitely caused

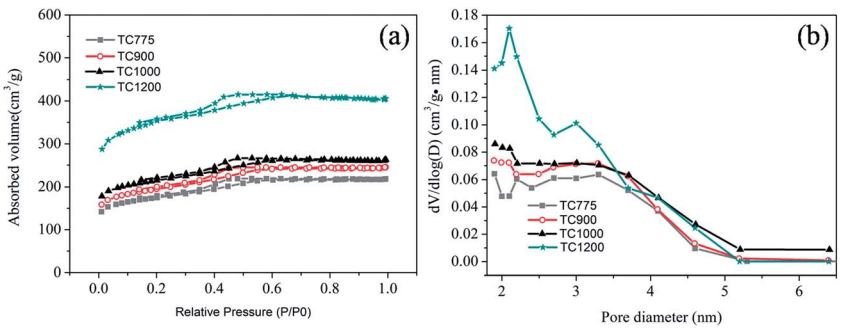

Fig. 2 (a) Nitrogen sorption isotherms of four samples TC775, TC900, TC1000 and TC1200 measured at 77 K and (b) the size distribution of mesopores calculated using the BJH method.

Table 2 Nitrogen sorption data for samples TC775, TC900, TC1000 and TC1200

Sample ID	S_{BET}, $m^2\ g^{-1}$	S_{meso}	S_{micro}	V_{meso}, $cm^3\ g^{-1}$	V_{micro}	D_{meso}, nm
TC775	603.4 ± 4.8	215.4 ± 3.3	377.1 ± 3.0	0.20 ± 0.01	0.28 ± 0.01	3.2 ± 0.2
TC900	670.7 ± 3.5	240.1 ± 4.2	439.2 ± 3.5	0.23 ± 0.01	0.32 ± 0.01	3.5 ± 0.1
TC1000	738.5 ± 5.1	257.2 ± 4.2	479.7 ± 3.0	0.24 ± 0.01	0.34 ± 0.01	3.8 ± 0.1
TC1200	1185.0 ± 4.5	340.6 ± 5.4	740.8 ± 4.1	0.80 ± 0.02	0.51 ± 0.05	4.3 ± 0.2

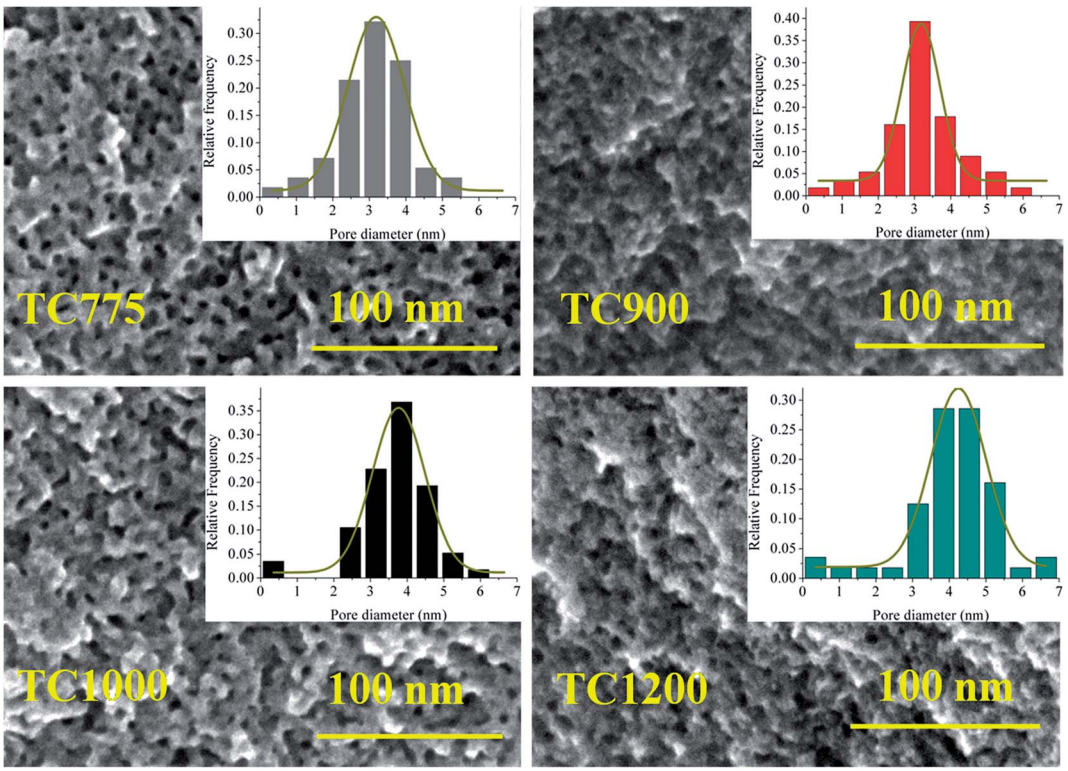

Fig. 3 SEM images of samples TC775, TC900, TC1000 and TC1200. Insets: the normal distributions of the pore diameter for each sample.

largely dropped density. Due to the synergistic effect of density, sample TC1200 will not be discussed on the sulfur impact on electrical conductivity.

The decreased conductivities of samples TC775, TC900 and TC1000 with increased pyrolysis temperature might be explained by the degree of graphitization of carbon network deteriorating, which is caused by the reaction between sulfur and carbon, preferentially, at lower temperatures. It is believed that sulfur reacts with imperfectly located carbon atoms to form CS_2 gas with heat treatment above 500 °C and then transfers these imperfect carbon atoms to perfect lattice positions, causing the improved degree of graphitization.[41] Heat treatment of the carbon at low temperatures is critical to make sulfur react with imperfect carbon atoms instead of sulfur evaporation without reaction.[42]

To ascertain this assumption, Raman spectroscopic tests were carried out to determine the graphitization degree through the peak intensity ratio of the D and G bands, which is denoted as $I(D)/I(G)$. A higher value of $I(D)/I(G)$ indicates a lower graphitization degree. The measured $I(D)/I(G)$ ratio followed the expectation that larger values of $I(D)/I(G)$ with higher temperatures. All samples had similar main features of graphitic materials, with D and G bands at ~1339 cm^{-1} and ~1589 cm^{-1}, respectively (Fig. 4c). The G band stems from in-plane vibrations and has E_{2g} symmetry. This is observed in all sp^2 carbon systems. The D band stems from a double resonance process involving a phonon and a defect. Due to the overlap of D and G bands, peak fitting was following the procedure outlined by Vallerot[43] to obtain additional information. Fig. 4c shows the fittings of additional bands associated with nanocrystalline graphitic materials as well as the standard D and G bands. Additional bands were labeled as D′, I and D″. The D′ band is ascribed to the defective graphitic systems and manifests as a shoulder on the G band at ~1620 cm^{-1}.[44] The I band is linked with disorder in the graphitic lattice, sp^2–sp^3 bonds or the presence of polyenes and is seen at ~1180–1290 cm^{-1}.[45,46] The D″ band (~1500 cm^{-1}) is known to occur in the presence of amorphous carbon.[47] Based on the fitting results, the $I(D)/I(G)$ values of TC775, TC900 and TC1000 were 1.17, 1.62 and 1.80 (Fig. 4b), respectively, showing that a lower value of $I(D)/I(G)$ was

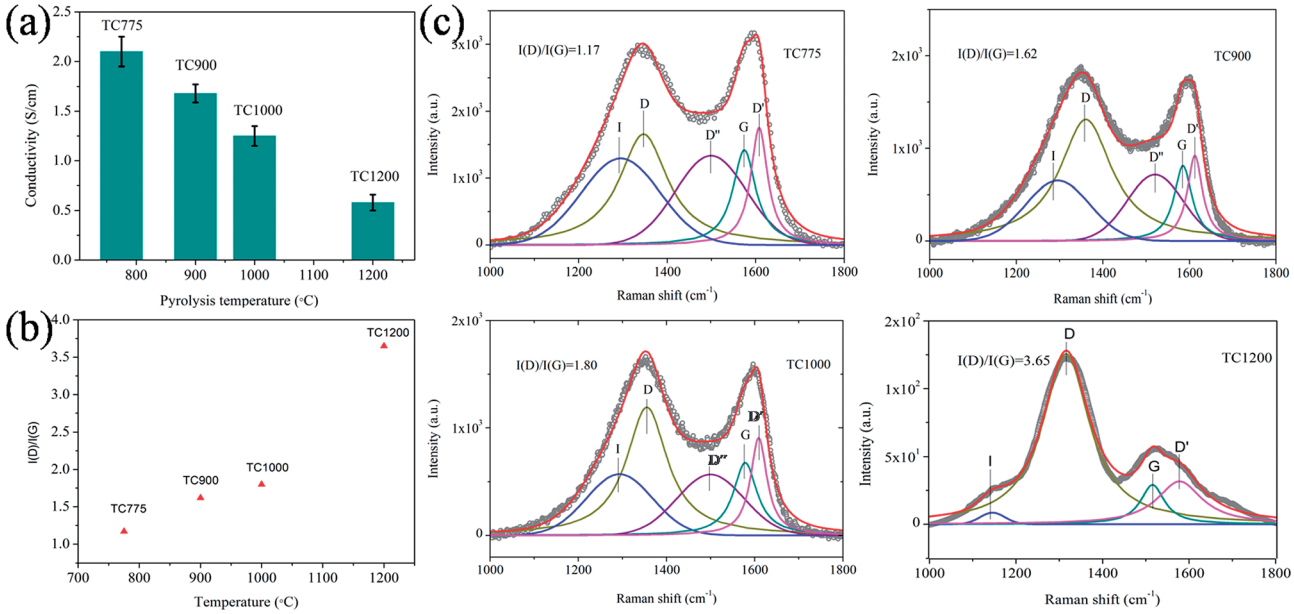

Fig. 4 (a) Summarized electrical conductivity of the TC samples. (b) The values of *I*(D)//(G) of the TC samples and (c) deconvoluted Raman spectra of TC samples showing D, G, D′, D″ and I bands.

obtained when lower pyrolysis temperature was employed. As a result, samples pyrolyzed at lower temperatures are likely to have higher graphitization degrees, which lead to the increased electrical conductivity.

3.3 Wettability

Table 3 summarizes contact angles of samples TC775, TC900, TC1000 and TC1200 with TEATFB in saturated 50–50 PC–DMC as testing liquid. Fig. 5a illustrates the images taken immediately when TEATFB in 50–50 PC–DMC liquid touched samples TC775, TC900, TC1000 and TC1200, respectively. Samples with increased pyrolysis temperature showed a trend of larger contact angles, implying deteriorated wetting behavior. According to the capillary model set to judge the wettability of the porous material, the wettability is determined by the capillary forces which caused by the stronger adhesive intermolecular forces between the liquid and a substance than the cohesive intermolecular forces inside the liquid. It is believed that the large pore size and intensive unit pore of radius are beneficial to enhance unit capillary forces of radius, which in turn makes the porous matrix soaking up the liquids.[48] It could be observed in BET results that the mesopore volume and mesopore size of TC samples all increased with soaring pyrolysis temperature. It should provide enhanced capillary forces, which pulls a wetting liquid so that it has a lower contact angle. However, the measurements show the reverse behavior from the changing trend of pores, with larger contact angles for more porous samples. As a result, the discrepancy in contact angles was attributed to modifying the carbon with different amounts of sulfur, rather than the pore structure. It should be noted that the solvent of the measuring liquid consists of PC and DMC, which are polar molecules. As shown in XPS analysis, in the TC samples sulfur atoms exist *via* the formation of the C–S bond to produce the thiophene-like structure. In this structure it can be proposed that a lone electron pair among the sulfur atom p-orbital overlaps with the π-orbital of the graphite sp^2 hybridization to form an extended π-system with a filled valence band (Fig. 5b). Thanks to a synergistic activation of conjugated carbon in combination with the electron-rich element S, a higher electron density is located at the surface of TC samples (compared to that of carbon without sulfur heteroatoms), leading to an increased dipole moment of the carbon matrix. The enhanced dipole moment enlarged the total polarization (*P*) of the medium,[23] which in turn facilitates the penetration of polar PC–DMC into pores according to The Like Dissolves Like Theory. As a result, a higher amount of sulfur is helpful to increase the wetting ability of the polar electrolyte into the carbon pores.

Table 3 Average contact angles measured immediately after the droplet touched the surface of the tested sheet. Sample TC775, which was pyrolyzed at 775 °C for 3 h, was completely wetted

Sample ID	TC775	TC900	TC1000	TC1200
Contact angle	Complete wetting	15.5° ± 1.1°	30.6° ± 0.3°	42.6° ± 1.4°

3.4 Electrochemical analyses

CVs taken at a scan rate of 10 mV s^{-1} are shown in Fig. 6a. The nearly rectangular shape of the CV curves of the TC samples indicates capacitive behavior from the formation of electrical double layers. TC775, TC900 and TC1000 also exhibited small, broad peaks in addition to the rectangular shape, suggesting pseudocapacitive reactions. However, broad peaks were hardly detected in TC1200, which shows that pseudocapacitance is not

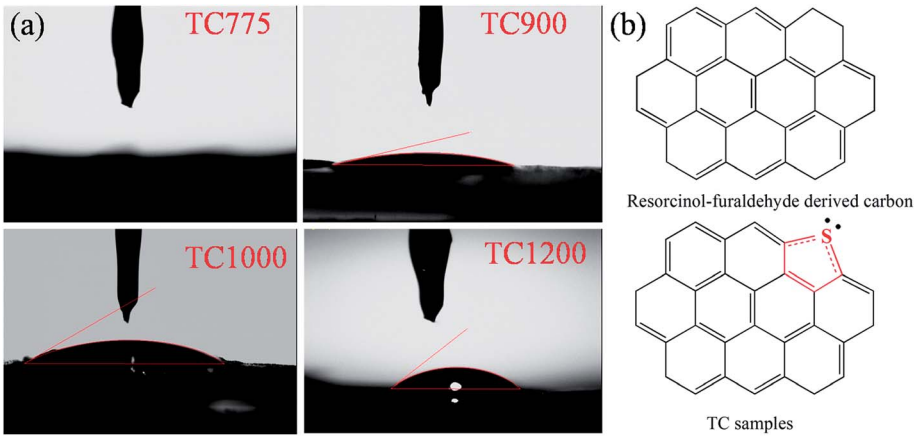

Fig. 5 Images showing the wettability of samples TC775, TC900, TC1000 and TC1200 samples. The uneven surfaces are from the edges of the sample rolling up and did not affect the measurement.

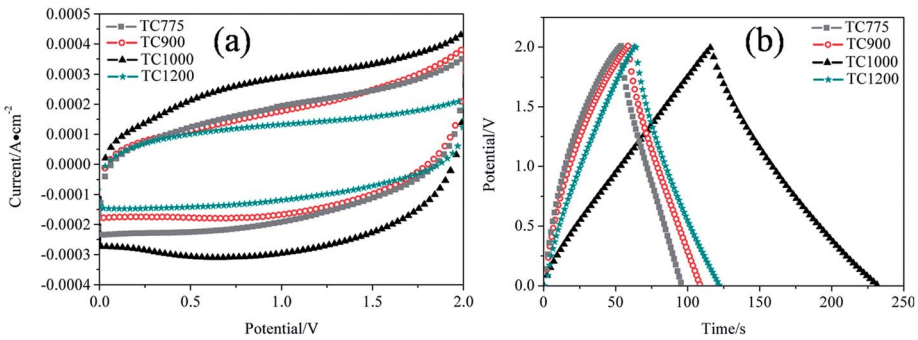

Fig. 6 CVs and GCs of samples TC775, TC900, TC1000 and TC1200.

obvious in this sample. From XPS results, the oxygen content of TC1200 is 5.0 ± 0.1 at% while that of TC1000 is 5.1 ± 0.1 at%, indicating that the appearance of broad peaks is not attributed to oxygen. It should be noted that the sulfur content of TC1000 (1.4 ± 0.1 at%) is around two times higher than that of TC1200 (0.5 ± 0.1 at%). Because there is no other element in the samples that can cause faradaic reactions except oxygen and sulfur, the pseudocapacitance can only be introduced by sulfur.

It is believed that pseudocapacitance arises from faradaic reactions induced by another lone electron pair from the sulfur groups interacting with the cations in the electrolyte. The following is a possible reaction that could be taking place:

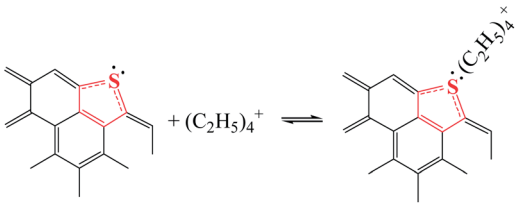

(2)

The specific capacitance was calculated from the discharge slopes of the galvanic cycling curves of the TC samples measured at 0.5 A g^{-1} (Fig. 6b), using eqn (1). The results are shown in Table 4.

Table 4 Capacitance based on mass, surface area, and volume

Sample ID	Specific capacitance (F g^{-1})	Capacitance based on total surface area (F m^{-2})	Volumetric capacitance (F cm^{-3})
TC775	4.6 ± 0.4	0.0076 ± 0.0007	2.22 ± 0.19
TC900	7.0 ± 0.5	0.0104 ± 0.0008	3.06 ± 0.22
TC1000	27.5 ± 0.5	0.0372 ± 0.0007	11.82 ± 0.21
TC1200	8.6 ± 0.5	0.0073 ± 0.0004	3.12 ± 0.18

With the increase in the pyrolysis temperature from 775 °C to 1000 °C, specific capacitance reaches the highest value (27.5 F g^{-1}) when carbon cryogel is pyrolyzed at 1000 °C. The value of specific capacitance had a drop when the pyrolysis temperature went up to 1200 °C. Even though the sulfur content dropped from 2.5 to 1.4 at% (~44% drop), the specific capacitance still increased nearly five times when the pyrolysis temperature increased from 775 °C to 1000 °C. Notably, in comparison with sample TC775, the micropore surface area of sample TC1000 increased nearly 100% with 40% increase in the mesopore surface area and 23% increase in the specific surface area. This result is in general agreement with published results for resorcinol–formaldehyde derived carbon aerogels.[49] An

enlarged surface area allows more sites for electrical double-layer formation. As discussed in Part 3.1, the enlarged mesopore volume is ascribed to the merging of micropores and these opened pores make the electrolyte readily diffuse, and dominate the performance of samples when the pyrolysis temperature is below 1000 °C. However, the effective impact of the pore structure on specific capacitance is not suitable for sample TC1200 with pyrolysis temperatures up to 1200 °C. Even though a 233.3% increase is in mesopore volume of TC1200 compared to that of TC1000, 53.6% drop in conductivity and nearly no pseudocapacitances co-intensify the degradation of specific capacitance. Fig. S5† shows the difference between specific capacitance and specific capacitance normalized to the surface area (SCS). The time value of each sample was based on its former sample with lower pyrolysis temperature. It can be clearly observed that with increased pyrolysis temperature, the values of SCS were always lower than that of specific capacitance, showing the deteriorated effect of the sulfur value drop on energy storage. However, difference in times between specific capacitance and SCS tended to be huge in sample TC1200 with drastic sulfur drop from 1.4 at% (TC1000) to 0.5 at%. Compared to other samples, SCS of TC1200 was only 0.19 times of TC1000 with 0.31 times specific capacitance based on sample TC1000. It can be illustrated that with an increased surface area of sample TC1200, the negative effect of sulfur drop can be compensated partially. But besides the surface area, the SCS reflected the realistically huge impact of the decreased amount of sulfur. When the sulfur content is above 0.5 at%, it can guarantee the contribution of pseudocapacitance and the sufficient amount of sulfur to effectively transfer incomplete carbon atoms. Thus, the main factor is the pore structure. In contrast, the sulfur content dominates the specific capacitance over the effect of the pore structure. The synergistic effect of pore structure, pseudocapacitance and electrical conductivity achieves the best level when the carbon cryogel pyrolyzed at 1000 °C, which shows the highest specific capacitance. When the capacitance is normalized to the surface area in these samples, TC1000 shows higher capacitance than that of TC1200, which is the same as the results of capacitance normalized to mass. It implies that sulfur can effectively increase the capacitance.

To confirm the sulfur effect on increasing capacitance of carbon matrix, a cell of pure porous carbon derived from RF resin was prepared and tested for charge–discharge at 0.5 A g^{-1} and for the CV test at a 10 mV s^{-1} scan rate. The SEM image (Fig. S6a†) showed that the prepared RF derived porous carbon had a similar pore morphology to that of sample TC1000. Nitrogen sorption isotherms of sample RF also exhibited type IV isotherms, similar to that reported in the literature.[30] It could be clearly observed in Fig. S6b† that there is no small, broad hump of the CV curve in sample RF compared to that of sample TC1000, indicating that no pseudocapacitive reactions existed in sample RF. Additionally, the specific capacitance normalized to the surface area of sample TC1000 was 4.8 times higher than that of sample RF, which indicated that obviously increased charges were stored per surface area in sample TC1000. It is found that the RF sample with the highest ratio value of I(D)/I(G), compared to that of all TC samples, further confirmed that the carbon transferring role of sulfur is to improve graphitization degree of carbon matrix and electron transfer ability. The pseudocapacitive reactions introduced from sulfur atoms enhanced by the improved electron transferring ability, raised the specific capacitance per surface area a lot.

The electrochemical stability of TC samples is shown in Fig. 7a. After 1000 cycles of charge and discharge, both materials did not show evident loss of capacitance (less than 4%), and sample TC1000 with 98.8% capacitance retention showed even better durability than other TC samples. Fig. 7b shows the last five charge–discharge cycles of TC1000. After long time cycling, sample TC1000 still maintained a good electrochemical reversibility with 99.2% Columbic efficiency. The good electrochemical stability of TC1000 can be ascribed to two parts: first, relatively larger mesopore size and volume than that of TC775 and TC900 enhance the organic electrolyte's mobility inside mesopores which prevents "trapped mesopores" from electrolyte filling in small size pores which are hard to be moved out; second, higher sulfur content compared to that of TC1200 improved the conductivity of the carbon matrix. Fig. 7c further reveals the current density dependence of the cycling performance of TC1000. During the first 200 cycles at 0.5 A g^{-1}, TC1000 shows a stable capacitance of ~27.5 F g^{-1}. In the following 600 cycles, although the charge–discharge rate changed successively, TC1000 always maintained stable capacitance. When the current density went back to 0.5 A g^{-1}, a fully recovered capacitance of ~27.5 F g^{-1} was obtained indicating that the TC1000 sample had excellent rate capability.

Electrochemical impedance spectroscopy provides further insight into how the pore structure, pseudocapacitance and conductivity are affecting the performance of samples. Nyquist plots are shown in Fig. 7d. Differences in surface charge resistance are evident at high frequencies, as seen in the inset. The changing trend of equivalent series resistance (ESR) is the same as that of specific capacitance. When pyrolysis temperature is below 1200 °C, the diameter of the semicircle at high frequency (an indication of charge transfer resistance) gradually decreased with raising pyrolysis temperature. However, when the pyrolysis temperature is 1200 °C, an increase was observed in the diameter of the semicircle. The charge transfer resistance is closely related to the surface area and pseudocapacitance as well as conductivity.[21,50,51] With increased pyrolysis temperature below 1200 °C, optimization of the pore structure with larger mesopore size and volume provides more active sites to form the double-layer, which overcomes the negative effect of less pseudocapacitance and lower conductivity. But when the sulfur content of TC1200 drops as much as 67% compared to that of TC1000, pseudocapacitance and conductivity dominate the process of charge transfer. At low frequencies, the slope of the curve shows the Warburg impedance which represents the electrolyte diffusion in the porous electrode host materials. TC1200 has the most ideal vertical line along the imaginary axis, which demonstrates that it has the lowest diffusion resistance. It should be noted that the slopes of curves in low frequencies become more inclined when the pyrolysis temperature decreased, which seems to be contradictory to the changing

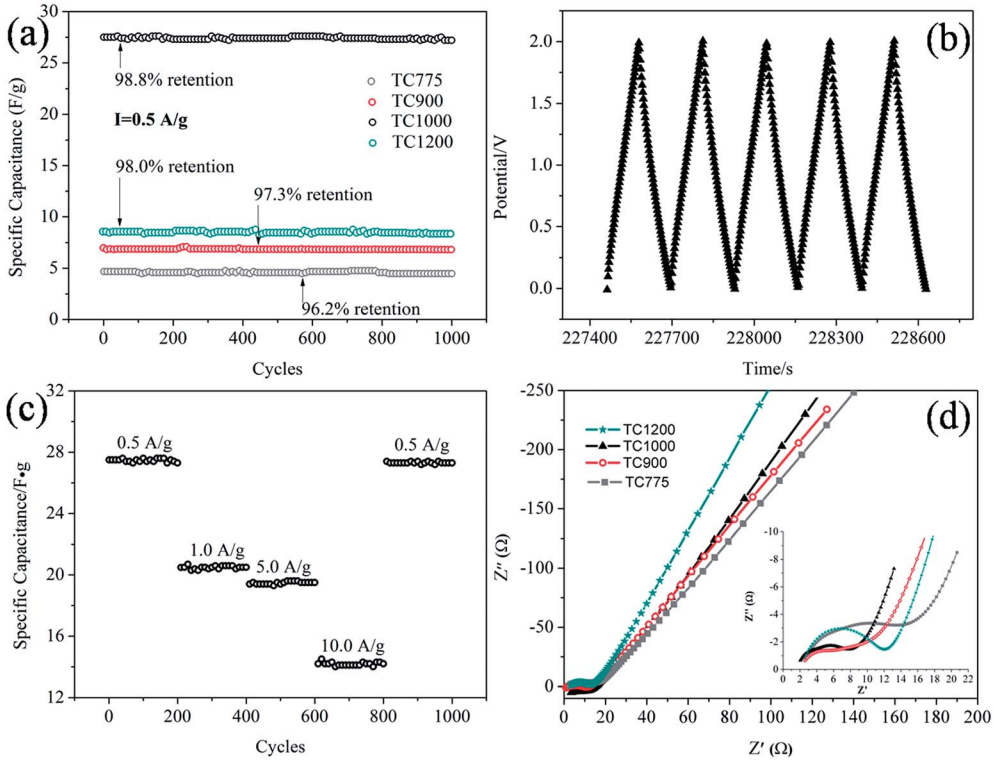

Fig. 7 (a) Cycling performance of TC samples with different pyrolysis temperatures tested under 0.5 A g^{-1} current density. (b) Last 5 charge–discharge curves of sample TC1000 which was pyrolyzed at 1000 °C with 0.5 A g^{-1} current density. (c) The current density dependence of sample TC1000. (d) Nyquist plots at high and low frequencies, inset. Sample TC1000 showed the highest capacitance despite a higher diffusivity resistance compared with sample TC1200.

trend seen for contact angles. In contact angle measurements, the data were collected immediately when liquid contacted the material surface. There was not enough time to make the liquid diffuse into pores thoroughly. On the other hand, impedance was measured after 10 cycles and pretreatment for 10 minutes at 2 V which makes the electrolyte penetrate into the pore instead of staying on the surface of the material. Additionally, in contact angle measurements, the existence of pores only enhances the effects of the applied surface chemistry without the real impact from the pore structure.[52] The contact angles illustrate more information of penetrating on surface chemistry rather than on the porous structure. Thus, more information on the pore structure is obtained in the low-frequency range of impedance even though there is a modification of the surface. In this sense, the enlarged mesopore size and volume facilitate the diffusion of the electrolyte ions through pores with increased pyrolysis temperature.

When TC samples were activated in air at 300 °C for 0.5 hours, both pore size and pore volume increased appreciably (Table 5). Consequently, the specific capacitance of TC1000 reached 94.4 F g^{-1} (Fig. 8), showing that such a sulfur-rich carbon cryogel has much potential to improve performance and is suitable for use as supercapacitors. There are more reports on the gasification effects on the optimization of the pore structure. The XPS result shows that with 0.5 h activation in air, the sulfur content just had a mild drop from 1.4 at% to 1.2 at%. It should be noted that the specific surface area of the activated

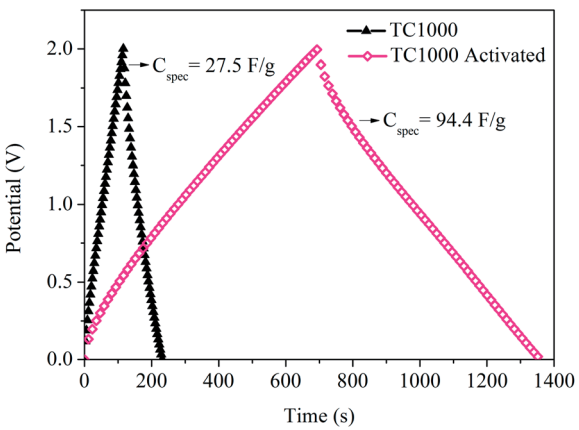

Fig. 8 GCs of sample TC1000 which was pyrolyzed at 1000 °C for 3 h and sample TC1000 after activation in air for 0.5 h.

sample increased nearly twice than that of sample TC1000 with increased mesopore size. It is well matched with the research studies on the gasification effect on porous carbon[53,54] that gas phase activation could enlarge the present pores. As mentioned previously, the increased specific surface area and mesopore volume will strongly improve the specific capacitance when the sulfur content is above 0.5 at%. Here, the doubled specific surface area makes increased accessible sites for forming a double-layer. The surface area of mesopore and mesopore size

Table 5 Nitrogen sorption data for sample TC1000 activated in air at 300 °C for 0.5 h

S_{BET}, $m^2\ g^{-1}$	S_{meso}	S_{micro}	V_{meso}, $cm^3\ g^{-1}$	V_{micro}	D_{meso}, nm
1105.0 ± 4.5	415.3 ± 4.0	582.6 ± 3.2	0.46 ± 0.01	0.40 ± 0.01	4.2 ± 0.2

rose causing more readily diffusion of the electrolyte into pores. The activation process helped the original TC samples to optimize the pore structure to improve carbon matrix properties. Meanwhile, such activation conditions can prevent the severe impact caused by a huge loss of sulfur (Table 5).

4 Conclusions

Sulfur was introduced by 2-thiophenecarboxaldehyde into a carbon matrix by sol–gel processing and has proved to induce faradaic reactions in organic electrolytes for supercapacitor applications. The capacitance loss of TC samples is less than 4% after 1000 charge–discharge cycles. Sample TC1000 pyrolyzed at 1000 °C can maintain 98.8% retention of the initial capacitance. Pyrolysis at low temperatures was found to retain more sulfur in the carbon. A 2.5 at% sulfur content dropped to 0.5 at% when the pyrolysis temperature increased from 775 °C to 1200 °C. High pyrolysis temperatures of sulfur-rich carbon were also found to result in carbons with high surface area, pore volume and large pore size in the mesopore regions. In addition, the graphitization degrees of carbon improved with thorough reaction between sulfur and imperfect carbon at lowered pyrolysis temperatures, which resulted in the increased electrical conductivity of TC samples. Furthermore, sulfur was found to be effective in improving the wetting behavior of carbon in organic electrolytes. An increased amount of sulfur in the carbon matrix made carbon more readily wetted due to the enhanced dipole moment of porous carbon. Specific capacitance and impedance were affected by synergistic effects of sulfur and the pore structure which made the TC1000 sample with 1.4 at% sulfur performs the best. When activated, the sulfur-modified carbon demonstrated a capacitance of 94.4 $F\ g^{-1}$ in organic electrolytes.

Acknowledgements

This work was supported in part by the National Science Foundation (NSF, CMMI-1030048). Yao Zhou also appreciates the sponsorship of the "Joint PHD program" of China Scholarship Council (CSC).

References

1 E. Frackowiak and F. Beguin, *Carbon*, 2001, **39**, 937–950.
2 D. W. Wang, F. Li and H. M. Cheng, *J. Power Sources*, 2008, **185**, 1563–1568.
3 *Electrochemical Supercapacitors: Scientific Fundamentals and Technological Applications*, ed. B. E. Conway, Kluwer Academic/Plenum Publisher, New York, 1999.
4 L. L. Zhang and X. S. Zhao, *Chem. Soc. Rev.*, 2009, **38**, 2520–2531.
5 A. G. Pandolfo and A. F. Hollenkamp, *J. Power Sources*, 2006, **157**, 11–27.
6 D. Hulicova-Jurcakova, A. M. Puziy, O. I. Poddubnaya, F. Suarez-Garcia, J. M. D. Tascon and G. Q. Lu, *J. Am. Chem. Soc.*, 2009, **131**, 5026–5027.
7 H. B. Wu, H. Pang and X. W. Lou, *Energy Environ. Sci.*, 2013, **6**, 3619–3626.
8 T. Y. Wei, C. H. Chen, H. C. Chien and S. Y. Lu, *Adv. Funct. Mater.*, 2012, **22**, 5038–5043.
9 D. W. Wang, F. Li, Z. G. Chen, G. Q. Lu and H. M. Cheng, *Chem. Mater.*, 2008, **20**, 7195–7200.
10 K. R. Prasad and N. Munichandraiah, *J. Power Sources*, 2002, **112**, 443–451.
11 C. Guan, J. P. Liu, C. W. Cheng, H. X. Li, X. L. Li, W. W. Zhou, H. Zhang and H. J. Fan, *Energy Environ. Sci.*, 2011, **4**, 4496–4499.
12 H. Q. Wang, Z. S. Li, Y. G. Huang, Q. Y. Li and X. Y. Wang, *J. Mater. Chem.*, 2010, **20**, 3883–3889.
13 G. H. Yu, L. B. Hu, N. Liu, H. L. Wang, M. Vosgueritchian, Y. Yang, Y. Cui and Z. N. Bao, *Nano Lett.*, 2011, **11**, 4438–4442.
14 S. L. Candelaria, R. Chen, Y. H. Jeong and G. Z. Cao, *Energy Environ. Sci.*, 2012, **5**, 5619–5637.
15 S. Sepehri, B. B. Garcia, Q. F. Zhang and G. Z. Cao, *Carbon*, 2009, **47**, 5996–6004.
16 K. Jurewicz, K. Babel, A. Ziolkowaski and H. Wachowaska, *Electrochim. Acta*, 2003, **48**, 1491–1498.
17 F. Beguin, K. Szostak, G. Lota and E. Frakowiak, *Adv. Mater.*, 2005, **17**, 2380–2384.
18 D. Hulicova-Jurcakova, M. Kodama, S. Shiraishi, H. Hatori, Z. H. Zhu and G. Q. Lu, *Adv. Funct. Mater.*, 2009, **19**, 1800–1809.
19 D. Hulicova, M. Dodama and H. Hatori, *Chem. Mater.*, 2006, **18**, 2318–2326.
20 Y. J. Kim, Y. Abe, T. Yanagiura, K. C. Park, M. Shimizu, T. Iwazaki, S. Nakagawa, M. Endo and M. S. Dressehaus, *Carbon*, 2007, **45**, 2116–2125.
21 S. L. Candelaria, B. B. Garcia, D. W. Liu and G. Z. Cao, *J. Mater. Chem.*, 2012, **22**, 9884–9889.
22 C. Portet, Z. Yang, Y. Korenblit, Y. Gogotsi, R. Mokaya and G. Yushin, *J. Electrochem. Soc.*, 2009, **156**, A1–A6.
23 G. Hasegawa, M. Aoki, K. Kanamori, K. Nakanishi, T. Hanada and K. Tadanaga, *J. Mater. Chem.*, 2011, **21**, 2060–2063.
24 X. C. Zhao, Q. Zhang, C. M. Chen, B. S. Zhang, S. Reichea, A. Q. Wang, T. Zhang, R. Schlogl and D. S. Su, *Nano Energy*, 2012, **1**, 624–630.

25 Q. G. Jiang, Z. M. Ao and Q. Jiang, *Phys. Chem. Chem. Phys.*, 2013, **15**, 10859–10865.
26 T. Y. Kim, H. W. Lee, M. Stoller, D. R. Dreyer, C. W. Bielawski, R. S. Ruoff and K. S. Suh, *ACS Nano*, 2011, **5**, 436–442.
27 D. S. Su and R. Schlog, *ChemSusChem*, 2010, **3**, 136–168.
28 M. S. Wu, T. L. Liao, Y. Y. Wang and C. C. Wan, *J. Appl. Electrochem.*, 2004, **34**, 797–805.
29 Y. X. Huang, S. L. Candelaria, Y. W. Li, Z. M. Li, J. J. Tian, L. L. Zhang and G. Z. Cao, *J. Power Sources*, 2014, **252**, 90–97.
30 B. B. Garcia, A. M. Feaver, Q. F. Zhang, R. D. Champion, G. Z. Cao, T. T. Fister, K. P. Nagle and G. T. Seidler, *J. Appl. Phys.*, 2008, **104**, 014305.
31 S. Glenis, A. J. Nelson and M. M. Labes, *J. Appl. Phys.*, 1999, **86**, 4464–4466.
32 S. R. Kelemen, M. Afeworki, M. L. Gorbaty, M. Sansone, P. J. Kwiatek, C. C. Walters, H. Freund and M. Siskin, *Energy Fuels*, 2007, **21**, 1548–1561.
33 N. Krishnankutty and M. A. Vannice, *Chem. Mater.*, 1995, **7**, 754–763.
34 M. E. Labib, J. H. Thomas and D. D. Embert, *Carbon*, 1984, **22**, 445–451.
35 K. E. Swider and D. R. Rolison, *Langmuir*, 1999, **15**, 3302–3306.
36 Y. H. Deng, T. Yu, Y. Wan, Y. F. Shi, Y. Meng, D. Gu, L. J. Zhang, Y. Huang, C. Liu, X. J. Wu and D. Y. Zhao, *J. Am. Chem. Soc.*, 2007, **129**, 1690–1697.
37 S. Tanaka, N. Nishiyama, Y. Egashira and K. Ueyama, *Chem. Commun.*, 2005, 2125–2127.
38 J. W. McBain, *J. Am. Chem. Soc.*, 1935, **57**, 699–700.
39 K. S. W. Sing, D. H. Everett, R. A. W. Haul, L. Moscou, R. A. Pierotti, J. Rouquerol and T. Siemieniewska, *Pure Appl. Chem.*, 1985, **57**, 603–619.
40 S. J. Kim, S. W. Hwang and S. H. Hyun, *J. Mater. Sci.*, 2005, **40**, 725–737.
41 M. H. Wagner, H. Pauls, H. Tillmans and G. Wilhelmi, *Ext. Abstr. 16th Biennial Conference on Carbon*, San Diego, CA, 1983, pp. 582–583.
42 S. R. Brandtzeg and H. A. Oye, *Carbon*, 1988, **26**, 163–168.
43 J. M. Vallerot, X. Bourrat, A. Mouchon and G. Chollon, *Carbon*, 2006, **44**, 1833–1844.
44 A. C. Ferrari, *Solid State Commun.*, 2007, **143**, 47–57.
45 W. S. Bacsa, J. S. Lannin, D. L. Pappas and J. J. Cuomo, *Phys. Rev. B: Condens. Matter Mater. Phys.*, 1993, **47**, 10931–10934.
46 N. McEvoy, N. Peltekis, S. Kumar, E. Rezvani, H. Nolan and G. P. Keele, *Carbon*, 2012, **50**, 1216–1226.
47 T. Jawhari, A. Roid and J. Casado, *Carbon*, 1995, **33**, 1561–1565.
48 X. Yao, Y. H. Hu, A. Grinthal, T. Wong, L. Mahadevan and J. Aizenberg, *Nat. Mater.*, 2013, **12**, 529–534.
49 S. A. Al-Muhtaseb and J. A. Ritter, *Adv. Mater.*, 2003, **15**, 101–114.
50 P. M. Biesheuvel, Y. Q. Fu and M. Z. Bazant, *Phys. Rev. E: Stat., Nonlinear, Soft Matter Phys.*, 2011, **83**, 061507.
51 X. Li and B. Q. Wei, *Nano Energy*, 2012, **1**, 479–487.
52 Y. L. Khung, M. A. Cole, S. J. P. mcInnes and N. H. Voelcker, Control over wettability *via* surface modification of porous gradients, *BioMEMS and Nanotechnology III*, ed. D. V. Nicolau, D. Abbott, K. Kalantar-Zadeh, T. Di Matteo and S. M. Bezrukov, SPIE, Bellingham, 2007.
53 P. V. Samant, F. Goncalves, M. M. A. Freitas, M. F. R. Pereira and J. L. Figueiredo, *Carbon*, 2004, **42**, 1321–1325.
54 N. Mahata, M. F. R. Pereira, F. Suarez-Garcia, A. Martinez-Alonso, J. M. D. Tascon and J. L. Figueiredo, *J. Colloid Interface Sci.*, 2008, **324**, 150–155.

